USAARL Report 86-4

THE BUSHBABY OPTIC NERVE: FIBER COUNT AND FIBER DIAMETER SPECTRUM

By
Jim E. Fulbrook
Loretta Peterson

SENSORY RESEARCH DIVISION

March 1986

USAARL

Notice

Qualified requestors

Qualified requestors may obtain copies from the Defense Technical Information Center (DTIC), Cameron Station, Alexandria, Virginia 22314. Orders will be expedited if placed through the librarian or other person designated to request documents from DTIC.

Change of address

Organizations receiving reports from the US Army Aeromedical Research Laboratory on automatic mailing lists should confirm correct address when corresponding about laboratory reports.

Animal use

In conducting the research described in this report, the investigators adhered to the Guide for Laboratory Animal Facilities and Care, as promulgated by the Committee on the Guide for Laboratory Animal Resources, National Academy of Sciences-National Research Council.

Disposition

Destroy this report when it is no longer needed. Do not return it to the originator.

Disclaimer

The views, opinions, and/or findings contained in this report are those of the author(s) and should not be construed as an official Department of the Army position, policy, or decision, unless so designated by other official documentation. Citation of trade names in this report does not constitute an official Department of the Army endorsement or approval of the use of such commercial items.

Reviewed:

BRUCE C. LEIBRECHT
LTC, MS
Director, Sensory Research
Division

Released for publication:

J. D. LaMOTHE, Ph.D.
COL, MS
Chairman, Scientific
Review Committee

DUDLEY R. PRICE
Colonel, MC
Commanding

SECURITY CLASSIFICATION OF THIS PAGE (When Data Entered)

REPORT DOCUMENTATION PAGE

READ INSTRUCTIONS BEFORE COMPLETING FORM

1. REPORT NUMBER: USAARL Report No. 86-4
2. GOVT ACCESSION NO.:
3. RECIPIENT'S CATALOG NUMBER:

4. TITLE (and Subtitle): The Bushbaby Optic Nerve: Fiber Count and Fiber Diameter Spectrum
5. TYPE OF REPORT & PERIOD COVERED:
6. PERFORMING ORG. REPORT NUMBER:

7. AUTHOR(s): Jim E. Fulbrook, Loretta Peterson
8. CONTRACT OR GRANT NUMBER(s):

9. PERFORMING ORGANIZATION NAME AND ADDRESS:
U.S. Army Aeromedical Research Laboratory
Fort Rucker, AL 36362-5000

10. PROGRAM ELEMENT, PROJECT, TASK AREA & WORK UNIT NUMBERS:
6.11.01.A
3A161101A91C 00 292

11. CONTROLLING OFFICE NAME AND ADDRESS:

12. REPORT DATE: March 1986
13. NUMBER OF PAGES: 43

14. MONITORING AGENCY NAME & ADDRESS (if different from Controlling Office):
U.S. Army Medical Research and Development Command
Fort Detrick
Frederick, MD 21701-5012

15. SECURITY CLASS. (of this report): UNCLASSIFIED
15a. DECLASSIFICATION/DOWNGRADING SCHEDULE:

16. DISTRIBUTION STATEMENT (of this Report):

17. DISTRIBUTION STATEMENT (of the abstract entered in Block 20, if different from Report):

18. SUPPLEMENTARY NOTES:

19. KEY WORDS (Continue on reverse side if necessary and identify by block number):
neuroanatomy
ultrastructural neuroanatomy
electron microscopy
optic nerve
bushbaby
Galago crassicaudatus
vision
axon diameter spectrum
image analysis

20. ABSTRACT (Continue on reverse side if necessary and identify by block number):
See back of form.

DD FORM 1 JAN 73 1473 EDITION OF 1 NOV 65 IS OBSOLETE

UNCLASSIFIED

SECURITY CLASSIFICATION OF THIS PAGE (When Data Entered)

20. ABSTRACT:

The number, percent myelinated, density, and size distributions of optic nerve axons in the bushbaby, Galago crassicaudatus, were estimated from a partial areal survey of cross-sectioned tissue examined by electron microscopy. The average of the data obtained by two experimenters yielded a total fiber estimate of 384,500 (±19,200). Unmyelinated axons comprised 2.8 percent of the population. The fiber density between peripheral and central optic nerve samples was homogeneous and estimated to be 376 fibers per 1000μm^2. Axon size distributions were distributed unimodally from 0.17-4.3 microns (mode=0.7). Unmyelinated axons ranged in size from 0.17-1.24 microns (mode=0.41). The comparative implications of these results are discussed in view of the bushbaby as a model for studies of human scotopic vision.

TABLE OF CONTENTS

LIST OF FIGURES

LIST OF FIGURES, Continued

LIST OF TABLES

INTRODUCTION

Vision depends on the orderly progression of complex neural events which originate in the photoreceptors and are transmitted in several successive stages, across several neural cell types enroute to the brain. The optic nerve is the bottleneck through which all sensory information about vision must pass. The number and size of the retinal ganglion cell axons comprising the optic nerve reflects the magnitude of the output of the retina and defines the "cables" or channels through which the environmental information of space, time, intensity, and sometimes, color must be transmitted and integrated. For this reason, since the earliest days of visual science, the optic nerve has been of particular interest to researchers. Thorough investigations of the neuroanatomy and electrophysiology of the retinal ganglion cell population and the axons of the optic nerve are necessary in the characterization of the visual system in any given vertebrate species. The purpose of this study is to provide a comparative neuroanatomical data base on the optic nerve of the bushbaby, Galago crassicaudatus, a nocturnal, prosimian primate and candidate preparation for scotopic or night vision research.

Since the earliest days of research on the vertebrate visual system, dozens of different species from amphibia to primates have been studied. These studies served two general purposes: that of comparative study to characterize the phylogenetic homologies, analogies, and specific differences between species, and the exploitation of particular animal preparations for having certain properties that allow for greater isolation and experimental control over other species. For instance, cold-blooded vertebrates are more readily used for intracellular recording from eyecup preparations because their retinal cells are larger and more easily penetrated than most vertebrates, and the tissue can remain viable for data collection for many hours longer than warm-blooded vertebrates.

The comparative findings on the vertebrate visual system have shown that while each species has significant anatomical and physiological differences in visual system organization, remarkable similarities in anatomy and in physiology are found among all vertebrates, particularly in retinal neuroanatomy and in the biochemical, biophysical, and neural coding properties of retinal cells. However, each research study still has limitations on its applicability across all the vertebrate classes and, conversely, much research on vision is designed for application to specific vertebrate models, especially humans.

One important area of human visual system function is that of scotopic or night vision. Most research conducted in this area has been done by human psychophysics paradigms under normal physiological conditions. Animal preparations used to study scotopic vision (dark adaptation, absolute threshold, etc.) have included cat (Harding and Enroth-Cugell, 1978), rat (Green, 1973), frog (Grusser and Grusser-Cornehls, 1976), and turtle (Granda and Dvorak,

1977). The skate, a cartilaginous fish, has been proposed as a preparation useful for studies of scotopic vision because its retina is nearly cone-free, but it is a poikilotherm with a comparatively primitive visual system (Dowling and Ripps, 1970; Green, et al., 1975). Ideally, an animal model for the study of scotopic vision in humans should be as close phylogenetically as possible to humans and have a nearly cone-free or rod-only retina. A retina that contained only rod photoreceptors would allow evaluation of scotopic mechanisms in complete isolation; however, to date, not one vertebrate has been shown to be exclusively cone-free in studies of electron microscopy or histochemistry, when many earlier research studies using only light microscopy had made such claims (Walls, 1942; Dartnall et al., 1965).

From all of the vertebrates studied thus far, the bushbaby retina appears to be one of the best candidates for electrophysiological, neuroanatomical, and neuropharmacological studies related to human scotopic vision (Casagrande and DeBruyn, 1982). The galago is a nocturnal, prosimian primate with a well-developed visual system. In addition, recent studies employing multiple neuroanatomical and histochemical techniques still have not been able to unequivocally identify cone photoreceptors in the retina, although a very small population of photoreceptors (estimated 1-4 percent) with many cone-like properties (Cohen, 1972; Rodieck, 1973) were identified (Hope and Ulshafer, 1984; Fulbrook, unpublished data). The primary drawback to the bushbaby as a scotopic model is that there is a sparsity of current, published research on the organization of its visual system (for reviews, see Casagrande and DeBruyn, 1982 and DeBruyn, Wise, and Casagrande, 1980). Here, we present a neuroanatomical survey of the optic nerve in the bushbaby to include an estimate of the total axon count, axon density and distribution, and an axon diameter spectrum determined by two experimenters working independently of each other with the same tissue and the same set of micrographs.

Quantitative and qualitative analyses of vertebrate optic nerves have been published on a wide range of vertebrates, especially on some of the more commonly used animals in vision research (cat: Stone and Hollander, 1971; Hughes and Wassle, 1976; Stone, 1978; Stone and Campion, 1978; rabbit: Vaney and Hughes, 1976; pigeon: Duff and Scott, 1979; rat: Hughes, 1977; turtle: Fulbrook and Granda, 1978; xenopus: Gaze and Peters, 1961; Peters, Palay, and Webster, 1970; Dunlap and Beazley, 1984). The techniques for conducting these studies are well established and fairly straightforward. However, most of the studies in the literature, to date, did not have the benefit of sophisticated digitized image anlaysis equipment in measuring cell areas and equivalent diameters. For example, most studies on size distributions employed circle templates to make subjective estimates of equivalent diameters for obliquely-shaped axons, and the tedium greatly limited the sample of axons and total nerve area that could be studied. This is one of the first research studies on optic nerves which has employed an advanced digitized image analysis system (Carl Zeiss Inc., Videoplan Image Analysis System)* to more accurately and rapidly collect, analyze, and collate data from electron and light micrographs of optic nerve tissue in cross section. This study contributes information to two areas in visual science:

*See Appendix A.

that of general comparative information on optic nerves in vertebrates and, more importantly, adds additional neuroanatomical information specifically to the growing body of literature on the bushbaby, Galago crassicaudatus, for its usefulness as an animal model of scotopic visual function.

MATERIALS AND METHODS

Tissue Preparation

One male and two female adult bushbabies, Galago crassicaudatus, weighing between 0.8-1.0 kg, were overdosed with 50-60 mg/kg intraperitoneal injections of Nembutal®. Once deep anesthesia was established, the animals were decapitated with a guillotine (Edco Scientific, Inc.)* and the optic nerves from just behind the optic disks, and including the optic chiasm, were gently dissected out of the cranial cavity. All dissection was carried out with the tissue bathed in a buffered fixative (3 percent glutaraldehyde in 0.1M phosphate buffer at pH = 7.4; Hyatt, 1981). The eyeballs and retinas of these animals also were dissected out for a different set of histological experiments that are not described here. The optic nerve from disk to chiasm is at least one centimeter long in the bushbaby.

Once removed, the pia mater and connective tissue surrounding the optic nerves were dissected away and the nerve was cut into 1 mm cross sectional lengths, excluding nearly 2 mm of optic nerve from just behind the optic disk and approximately 2 mm of nerve preceding the optic chiasm. The samples were then placed in 3 percent buffered glutaraldehyde fixative for three hours at 0° C. After a buffer wash, the tissue was postfixed with 1 percent osmium tetroxide, in 0.1 M phosphate buffer for three hours at 0° C (Hyatt, 1981). The tissue was dehydrated at room temperature using a graded series of acetone solutions (30%, 50%, 70%, 95%, 100%), then infiltrated and embedded with Spurr, low-viscosity, epoxy embedding medium (Polysciences, Inc.)*. Infiltration took place over two days with polymerization and hardening occurring over an additional 24-hour period in an oven at 65° C.

The tissue was embedded in flat-mounted molds for square ultramicrotome chucks. Small paper labels were placed with the oriented tissue (longitudinal and cross sectional orientations) in each block for identification and reference. Tissue blocks were stored in a desiccant, then trimmed or "faced" into trapezoids with edges up to 1.5 mm long to include the entire nerve.

Light and Electron Microscopy

Both thick and ultrathin sectioning was accomplished on a Sorvall MT-5000 Ultra Microtome*. Thick sections from 0.5-1.0 μm were cut and

mounted onto glass slides, then stained for up to five minutes in 0.1 percent toluidine blue, in 1 percent aqueous sodium borate (Hyatt, 1981). These sections were used for checking tissue orientation and light microscopy observation of whole nerves. Observations and photomicrographs were made using a Leitz Orthoplan light microscope*, at low powers with 6.3-25X planapo objectives or under oil immersion with a 40X planapo objective.

Ultrathin sections from 60 - 90 nm (gold to silver interference colors) were taken from the ultramicrotome and placed on Pelco, Inc. 300 mesh grids. Tissue grids were stained for 10 minutes with saturated uranyl acetate in 50 percent ethanol (Epstein and Holt, 1963), then stained again for 25 minutes with lead citrate (Reynolds, 1963). After washing with distilled water and drying on filter paper, the grids were stored in labeled holders or inserted and viewed in the electron microscope.

A Carl Zeiss, Inc., EM10C electron microscope* operating at 60 kV was used for ultrastructural observation. Observations were made at magnifications of 2,300X, 3,150X, 5,000X, and 6,300X. Photomicrographs were taken using Kodak 4489 electron microscope film (3.25 x 4 inches)*. Electron micrographic negatives were enlarged to yield final print magnifications of 7,500X, 9,450X, 15,000X, and 18,900X for data collection and analysis.

Tissue in the electron microscope was observed, identified, and photographed from two easily recognized optic nerve regions: central and peripheral. Once an area of optic nerve was defined, a montage strip of electron micrographs was taken from within a grid area by quasirandomly moving the grid stage of the electron microscope in one direction. No attempt was made to avoid nonneural areas from within the montage strips of optic nerve. Avoiding nonneural areas would bias the whole nerve density estimates of fibers to the high side. A sample of up to 30 micrographs could be collected from within one grid area. From these samples, over 100 electron micrographs of optic nerve in cross section were assembled into two identical sets for sampling and analysis by two independent experimenters.

Axon Identification and Analysis

Our criteria for the identification of nerve fibers in cross section were the same as those established and used in previous studies (Peters, 1966; Hughes and Wassle, 1976; Rhoades, Hsu, and Parfett, 1979). Myelinated axons are rather easily discriminated because of the encirclement of the axon by the myelin sheath. Within any axon it is possible to further recognize such characteristic organelles as neurofilaments, microtubules, mitochondria, and smooth endoplasmic reticula. Shrinkage and preservation of axoplasm ultrastructure was variable in quality and parts of the sheath showed some breakdown or unraveling of lamellae in some myelinated cells; but, these factors did little to interfere with the tracing of axon areas from just within the dark edge or internal mesaxon ring of the myelin sheath. This study did not make any measurements of the myelin sheath thickness, count the number of lamellae, or include the myelin sheath in fiber diameter estimates as have some other studies (Ogden and Miller, 1966; Tiao and Blakemore, 1976;

Rhoades, Hsu, and Parfett, 1979). This study describes measurements, densities, and counts of only the clearly recognizable axons and axon areas.

The presence of axons with diameters as small as 0.2 microns is well established in the literature. Identification of fibers this small required a minimum print magnification of 7,500X, although magnifications between 10,000-15,000X made identification easier and more reliable.

The myelin sheath provides a single high-confidence criterion in identifying these fibers, but unmyelinated axons can be very difficult to discriminate. The identification of unmyelinated axons was based primarily on the shape of the axon, its membrane thickness, and the axoplasmic contents (Maturana, 1959, 1960). The differentiation of unmyelinated axons from myelinated axons sectioned at a node of Ranvier was based on the presence of electron densities and granular substance around the axolemma of the axon in the paranodal region of myelinated cells (Peters, 1966).

Fibrous astrocytes characteristically have long-ranging processes in the form of membrane-bound fascicles or bundles of neurofilaments about the size of an unmyelinated axon. When cut in cross section these processes could easily be mistaken for unmyelinated axons. Astrocytic neurofilament processes and "end-feet" are highly concentrated in the periphery of the optic nerve which makes discrimination of unmyelinated axons even more difficult in that region. Whenever there was difficulty in distinguishing an unmyelinated axon from a neuroglial process or node of Ranvier, the feature was not counted. Unmyelinated axons were counted and measured by only one of the experimenters in this study. While a small population of unmyelinated fibers can be clearly and reliably identified in the bushbaby, the representation and, especially, the distribution in the optic nerve has a much lower subjective confidence interval compared to the myelinated fiber data in this study.

Compression of tissue from thin sectioning has been shown to occur and has been corrected for in some studies (Vaney and Hughes, 1976; Rhoades, Hsu, and Parfett, 1979). Estimates and measurements of compression in tissue, which would lead to underestimates in axon size, ranged from 2-9 percent in the studies cited. Tissue compression was not calculated in this study, although it is easy to recognize in micrographs whenever most of the axons appear elongated in the same direction. Micrographs with tissue regions like the above were discarded from the data set. No corrections for potential shrinkage from histological processing were made in this study.

It is well established from the earliest studies of the optic nerve that axons are not rigid, circular tubes (Maturana, 1959). They do not traverse the length of the optic nerve in register with each other but, rather, take a sinuous path enroute to their destinations (Bunt and Horder, 1983). Hence, many axons seen in cross sectional micrographs actually are cut in transverse section, which would yield an overestimate of their actual size. It is not possible to tell which elongated axons were cut in cross or transverse section, so corrections could not be made. Oblique fibers adjacent to circular fibers or other oblique fibers with long axes orthogonal to each other were evidence for occasional transverse sectioning rather than compres-

sion. However, it is fortuitous that the overestimation of axon size that occurs from transverse-sectioned axons is, to some degree, compensated by the under-estimates that would occur from tissue shrinkage and compression.

Even with defined criteria for identifying and measuring axons, subjective differences in data collection between experimenters would not be surprising. Hence, two experimenters analyzed most of the same micrographs without the benefit of any interaction or comparison of measurement criteria on partial results.

Computer Image Analysis

All of the micrographs were analyzed by being measured over a digitized tablet field of a Zeiss Videoplan Image Analysis System. The initial analysis process involved entering the micrograph identification and setting the appropriate magnification scale. Different identification parameters allowed for the separation of data files taken from the central and peripheral nerve areas. Figure 1 shows an example of an electron micrograph and the data acquired from tracing each axon with a cross-hair cursor. The axons in the photograph are numbered for ease of explanation. The data acquisition parameters in this study included measurements of axon area and calculation of an equivalent diameter, called DCIRCLE. Separate channels (0-3) were selected for data collection and storage. The entire area of the photomicrograph was measured and stored in channel 0 (46.535 square microns in Figure 1B). Measurements of each of the complete myelinated axons then were taken and stored in Channel 1 (axons numbered 1-21 in the photograph).

Channel 2 was used to count and store incomplete myelinated axons. In Figure 1, all of the incomplete axons were counted (22-40); but, in actual data collection, only those axons along 50 percent of the photographic edge of neural tissue would be counted (cells numbered 22-33 in the figure). Whenever a grid bar or outside nerve border was visible in a micrograph, that area was not counted in any area estimates or in making incomplete axon counts. Since each micrograph region was quasi-randomly selected, the probability was 50 percent that each incomplete cell represented half or less of its total area and half of the total edge count. To account for the area of the uncounted cells, the counted axons had its area doubled by the image analysis program for later cell density analyses. Unmyelinated axons were measured and stored in Channel 3. No examples are shown in Figure 1. Figure 1B shows the selected channel, raw count, and area and equivalent diameter measurements the image analysis system printed out after each of the axons were traced. Figure 1C shows a printout of the tracing of each cell and the photograph border. While the printed display of the traced axons shown in Figure 1C is not in scale with the actual data, the video monitor image displayed during data acquisition was in approximate scale. The video monitor and printed displays both had far less resolution than the active field of the digitizer tablet on which tracings were made.

Once all of the electron micrographs were analyzed, the data could be collated and displayed with considerable user control. In this study, most of the statistics and all of the data graphs and tables were generated by the evaluation programs of the image analysis system. Data have been rounded off to three decimal places. Data graphs in the RESULTS show the separate and combined experimenter results of the myelinated and unmyelinated axon size distributions for central and peripheral optic nerve regions.

RESULTS

Light Microscopy

Observations of thick sections of the bushbaby optic nerve revealed an oval-shaped whole nerve of densely packed myelinated nerve fibers (Figure 2). Blood vessels can be seen within the optic nerve, but most are found along the outer edge of the nerve associated with prominent invaginations of connective tissue into the nerve proper. A prominent blood vessel and invagination can be seen in the ventral portion of the optic nerve, likely representing the central branch of the ophthalmic artery (Figure 3). The connective tissue invaginations and septa divide the optic nerve into many fascicles, but not as discretely as in many vertebrates (cat: Stone and Campion, 1978; turtle: Fulbrook and Granda, 1978). The cross-sectioned optic nerves ranged in length from 1.25 to 1.3 mm along the longest (horizontal) axis. The average cross sectional area of optic nerve was 1,022,200 μm^2 ($\pm$35,000 μm^2). Light microscopy also revealed a significant population of light- and dark-staining neuroglial cells, usually associated with connective tissue invaginations (Figure 4). Myelinated axons, readily seen throughout the central and peripheral optic nerve regions, are commonly oblique and circular, have a considerable size range, and appear to be uniformly distributed.

Electron Microscopy

General survey electron micrographs of the bushbaby optic nerve are shown in Figures 5-7. The edge of the optic nerve is composed mainly of longitudinal and orthogonal collagen arrays, melanin pigment granules, blood vessels, and other connective tissue cells. A border of astrocytic foot processes separates all connective tissue from other neural tissue throughout the nerve (cf, Figure 5). A typical astrocyte nucleus and neurofilament process can be seen interdigitating the densely packed myelinated fibers in Figure 6. Oligodendrocytes, recognized mainly by dark-staining nuclear chromatin, also are found throughout the optic nerve, although astrocytes appear to outnumber the oligodendrocytes, especially in the central region of the optic nerve. The larger myelinated axons usually were more oblique than the smaller axons and there was a tendency for the larger fibers to have thicker myelin sheaths.

FIGURE 1. A: Electron micrograph of optic nerve in cross section. Tissue stained in uranyl acetate and lead citrate, magnification = 25,200X. Calibration bar is 1 m. Axons are numbered for ease of explanation. B: Sample of data measured by tracing each axon in "A" along the inside of the myelin sheath. Identification, parameter selection, and information extensions initially are chosen by the experimenter and appear in the first row of text. The storage channel, count, measured area, and calculated equivalent diameter (DCIRCLE) are given for each traced axon. C: Data print of the traced axons from "A" and the photograph border. See Methods text for additional details.

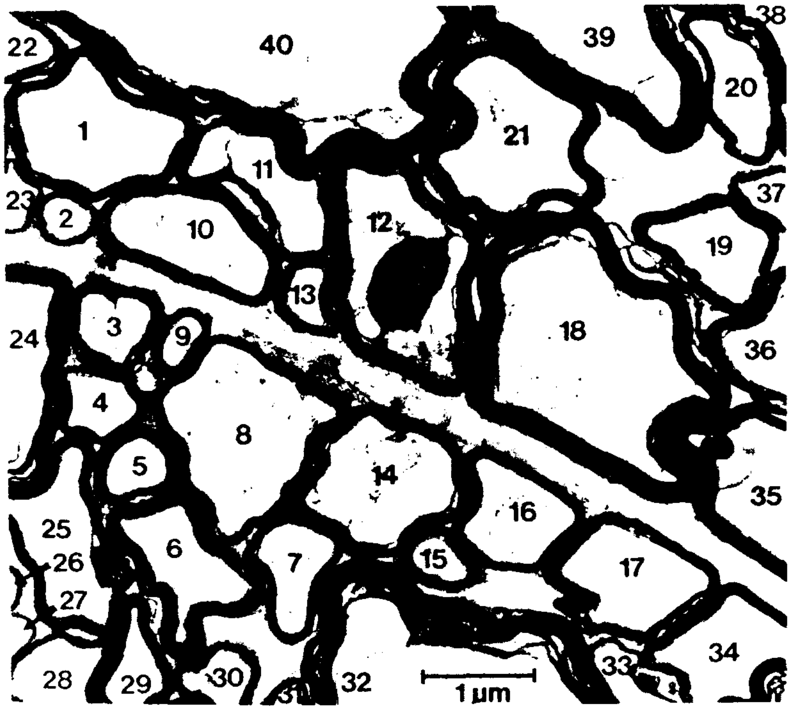

IDENT NR. JFBB01 01 99 CNVERT MAG=25200..2PTTRANS=0.795..11FEB85

CHAN	COUNT	AREA	DCIRCLE
0	1	46.535	7.697
1	1	1.119	1.194
1	2	.125	.398
1	3	.314	.633
1	4	.257	.572
1	5	.211	.519
1	6	.567	.850
1	7	.412	.725
1	8	1.572	1.415
1	9	.111	.376
1	10	.816	1.019
1	11	.720	.958
1	12	1.615	1.434
1	13	.161	.452
1	14	1.097	1.182
1	15	.149	.436
1	16	.617	.886
1	17	.819	1.021
1	18	2.628	1.829
1	19	.569	.851
1	20	.508	.804
1	21	1.241	1.257
2	1	.158	.449
2	2	.106	.368
2	3	.568	.851
2	4	.844	1.037
2	5	.013	.130
2	6	.045	.239
2	7	.367	.680
2	8	.242	.555
2	9	.219	.527
2	10	.039	.223
2	11	1.674	1.460
2	12	[illegible]	.475
[illegible]	13	[illegible]	[illegible]
[illegible]	14	[illegible]	[illegible]
[illegible]	15	[illegible]	[illegible]
[illegible]	16	[illegible]	[illegible]
[illegible]	17	[illegible]	[illegible]
[illegible]	18	.438	[illegible]
[illegible]	19	[illegible]	[illegible]

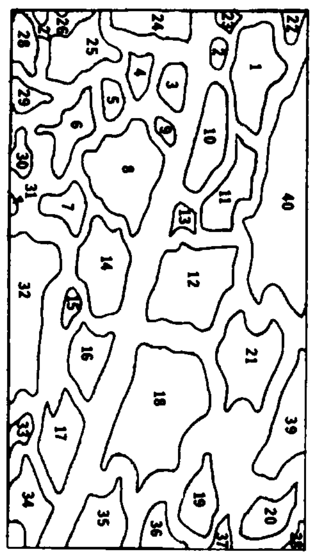

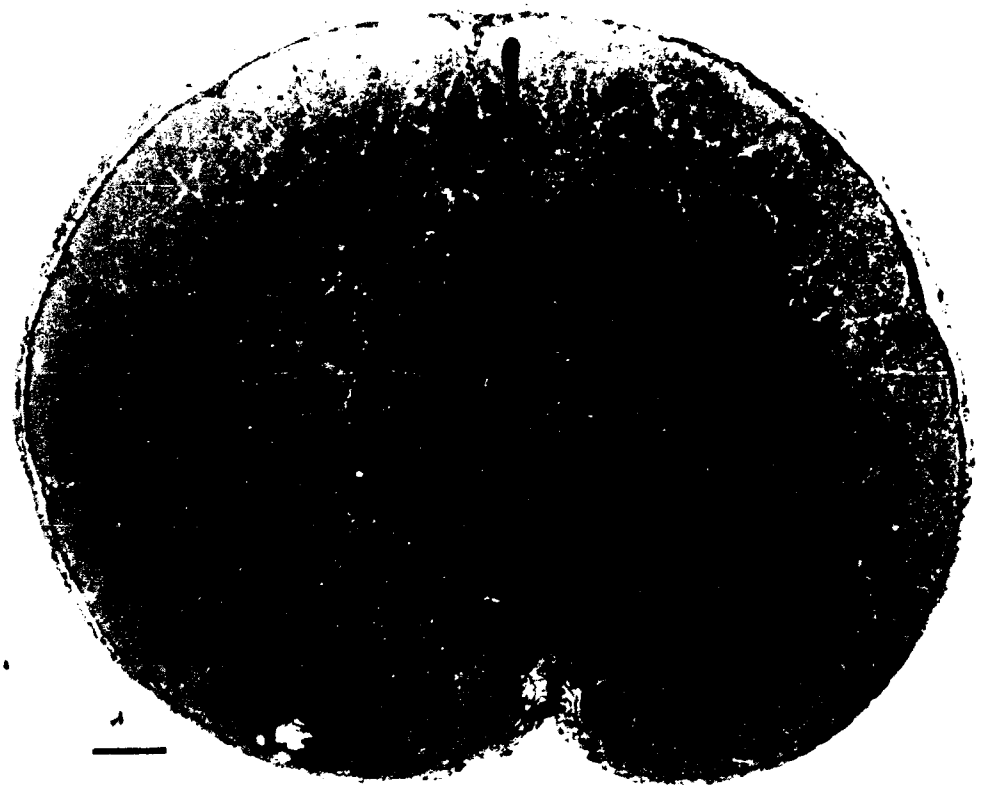

FIGURE 2. Light micrograph of whole optic nerve in cross section. Section stained in toluidine blue. Calibration bar is 100 microns, magnification = 100X. A prominent blood vessel is seen in the ventral portion of the optic nerve and many canal-like invaginations and processes are visible throughout the tissue section.

FIGURE 3. Light micrograph of a prominent blood vessel and connective tissue invagination in the ventral portion of optic nerve. Several dark-staining nuclei (oligodendrocytes) are visible among the densely packed myelinated fibers. Cross section stained in toluidine blue, magnification = 800X. Calibration bar is 10 m.

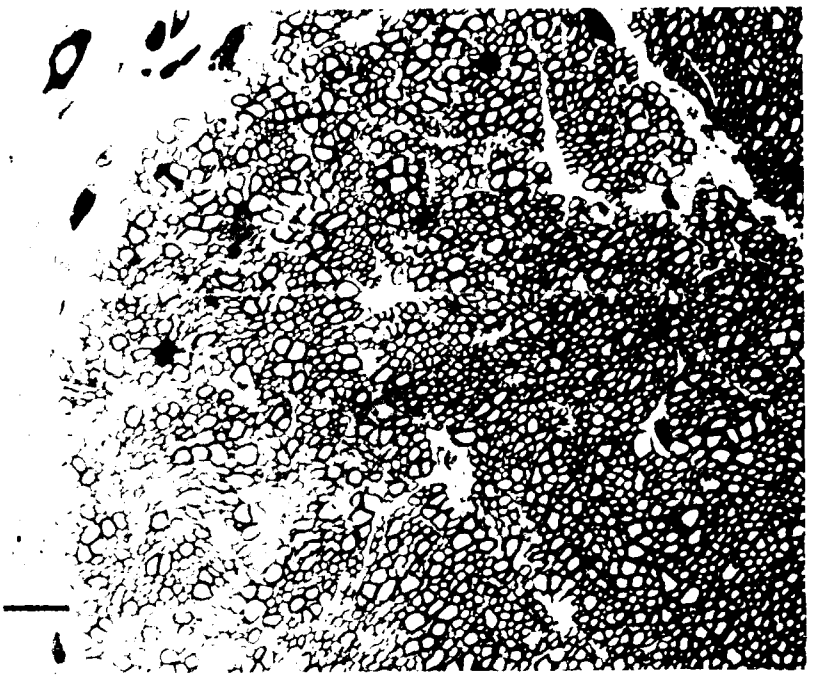

FIGURE 4. Two light micrographs of optic nerve in cross section. Tissue stained in toluidine blue, magnifiction = 800X. Calibration bars are 10 m. A: General survey micrograph of peripheral optic nerve. B: General survey micrograph of central optic nerve. Densely packed myelinated fibers, dark- and light-staining nuclei, and canals or channels of connective tissue and astrocyte processes are visible in both micrographs.

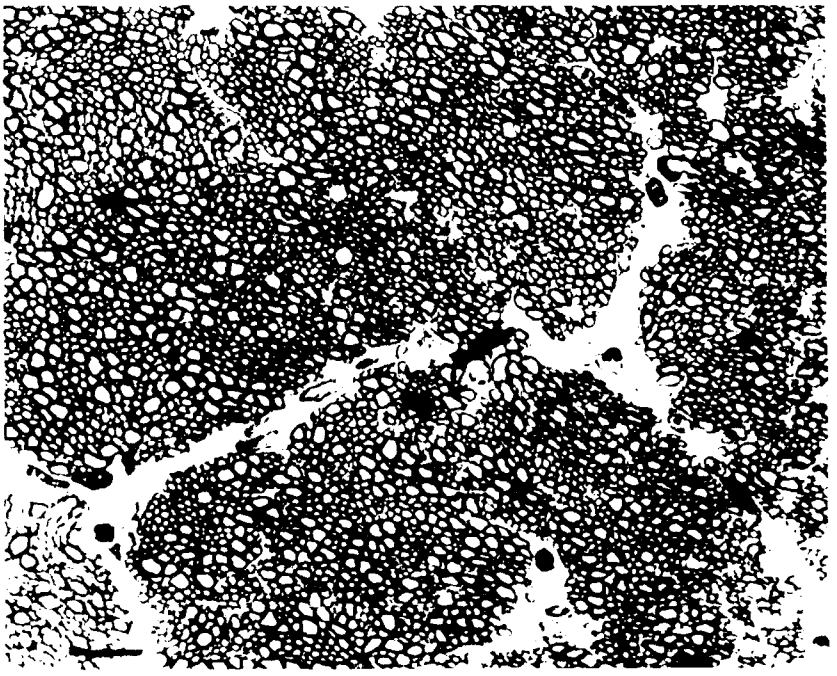

Axoplasmic organelles to include neurofilaments, microtubules, and mitochondria are readily visible within the axons. Figure 7 shows a grouping of four unmyelinated axons. These axons usually were found proximal to astrocyte nuclei as shown here and usually were found singly rather than in bundles or fascicles as in most vertebrates (turtle: Fulbrook and Granda, 1978; pigeon: Binggelli and Paule, 1969; frog: Maturana, 1959).

Nerve Fiber Total Counts and Density Distribution

A Pearson product-moment correlation coefficient test was performed on the myelinated fiber totals found by each experimenter on the individual photomicrographs done in common (n=60). This yielded an r=0.998 which demonstrated considerable agreement between experimenters on axon identification and counting. The total number of fibers in the bushbaby optic nerve was obtained by dividing the total nerve area (1,022,000 μm^2) by the total sample area (79,888 μm^2), then multiplying the quotient by the total cell count (30,046). This yielded a pooled estimate of 384,500 (±19,200) total fibers calculated from a sample of 7.8 percent of a total nerve. The pooled data from both experimenters yielded an average axon density of 376 fibers per 1000 μm^2. Unmyelinated axons comprised 2.8 percent of the axon population. The fiber density between the peripheral and central optic nerve samples was found to be statistically homogeneous allowing the total number of nerve fibers to be pooled. See Table 1 for a summary of experimental results on fiber counts, area, and density.

Axon Size Distributions and Experimenter Comparisons

The series of results on equivalent diameter distributions of central, peripheral, and combined optic nerve areas for both experimenters are shown in Figures 8 through 17. Each of the figures gives the absolute frequency histograms, and the classification listing for the data. Data are displayed with a bin-width interval of 0.2 microns over the range of 0.0-4.0 or 4.4 microns. The count, mean, standard deviation, median, and mode are given in the histogram for each of the figures. The diameter distributions and counts for myelinated fibers (Figures 8-14) are collated only from the population in which the complete axon could be traced (Channel 1 data).

Myelinated axons ranged in size from 0.17 microns to 4.3 microns in diameter, but the great majority fell between 0.4-1.6 microns. The mean myelinated fiber size for the pooled data was 1.07 microns with a modal value of 0.708 (Figure 8). All of the data samples were unimodal and positively skewed toward the larger fiber sizes.

Two-sample or matched-pair t-tests were performed on the peripheral and central optic nerve samples, and between experimenters on the pooled results. In general, all of the sample pairs tested were statistically the same (p .05). Only two statistically significant (p 0.05) differences were found: between the mean myelinated fiber size results of experimenter 1 and experimenter 2, and between the population sizes of unmyelinated

FIGURE 5. Electron micrograph of outside border of optic nerve and connective tissue sheath. Cross section stained in uranyl acetate and lead citrate, magnification = 10,250X. Calibration bar is 1 m. A blood vessel nucleus and lumen (L) are visible in the upper left-hand corner. Longitudinal collagen (C) arrays and melanin are seen proximal to the neural border. The neural border is composed of astrocyte foot-processes (A). Myelinated axons were never seen to abut any connective tissue without an astrocyte process in between.

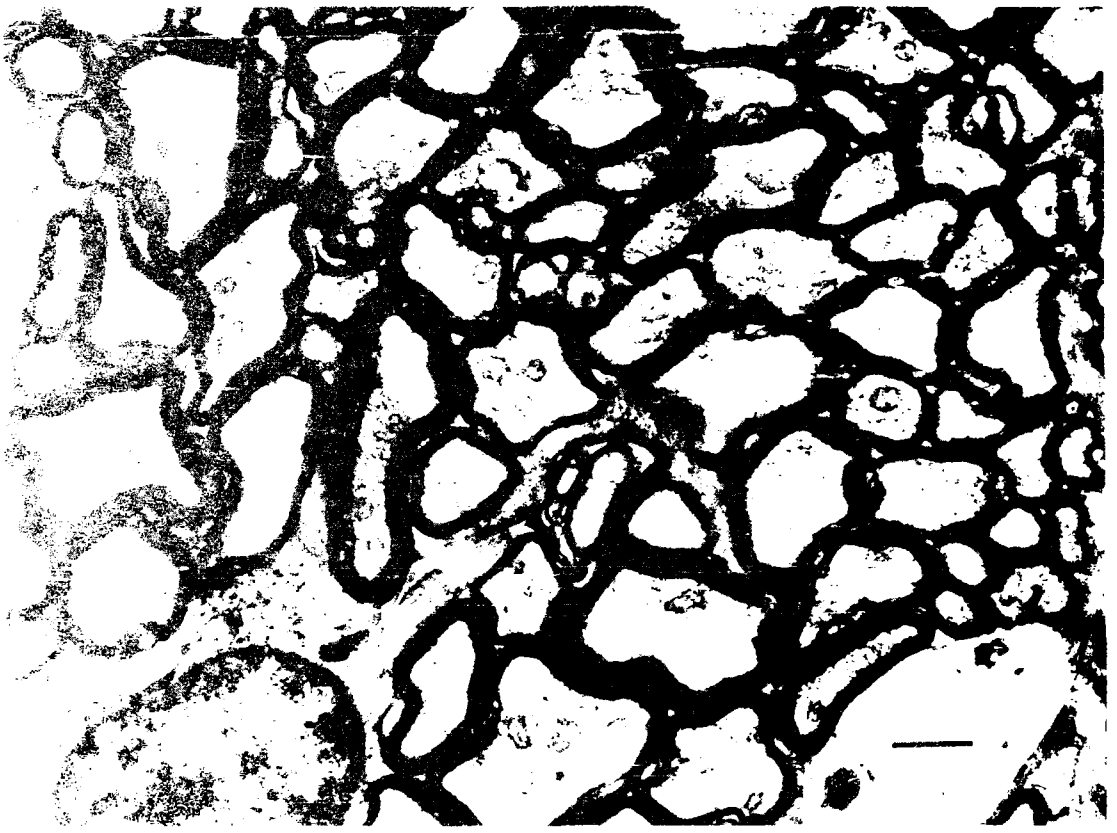

FIGURE 6. Electron micrograph of central optic nerve in cross section. Tissue stained in uranyl acetate and lead citrate, magnification = 10,250X. Calibration bar is 1 m. Myelinated fibers of various shapes, orientations, and sizes easily are discriminated. An astrocyte nucleus is seen in the lower left-hand corner of micrograph. Several astrocyte neurofilament processes can be seen, especially an enlarged region of neurofilaments in the lower right-hand corner.

FIGURE 7. Electron micrograph of optic nerve in cross section. Tissue stained in uranyl acetate and lead citrate, magnification is 10,250X. Calibration bar is 1 m. Four unmyelinated axons are shown in the para-nuclear region of an astrocyte. Neurofilament processes are numerous around astrocyte nuclei. Note the difference in shrinkage and unraveling of myelin between myelinated fibers in the upper right-hand corner of micrograph.

TABLE 1

SUMMARY OF EXPERIMENTAL RESULTS

Factor	Experimenter 1	Experimenter 2
Sample Area (μm^2):		
Total:	35,294	44,594
Central Optic Nerve:	18,540	23,453
Peripheral Optic Nerve:	16,754	21,141
Myelinated Fiber Counts:		
Total:	13,479	16,567
Central Optic Nerve:	7,456	9,080
Peripheral Optic Nerve	6,023	7,487
Unmyelinated Fiber Counts:		
Total:	382 (2.8% of pop.)	---
Central Optic Nerve:	239 (3.1% of pop.)	---
Peripheral Optic Nerve:	143 (2.3% of pop.)	---
Percent of Whole Nerve Sampled:*		
Total:	3.45	4.36
Central Optic Nerve	1.81	2.29
Peripheral Optic Nerve	1.64	2.07
Total Fiber Count:*	390,385	379,755
Fiber Density:*	382/1000 μm^2	372/1000 μm^2

*Based on an average whole nerve area of 1,022,200 μm^2.

axons in the peripheral and central optic nerve regions. Results of experimenter 1 (cf, Figure 9) showed a mean equivalent diameter of myelinated fibers equal to 1.05 microns (mode = 0.70 microns); experimenter 2 (cf, Figure 12) had a mean axon diameter size of 1.10 microns (mode = 0.716). Even though the differences are statistically significant, the actual difference in axon size estimates of only 0.05 microns between experimenters is trivial.

A small percentage of features recognized as unmyelinated axons by having met all recognized identification criteria were clearly and reliably encountered. These axons represented 2.76 percent of the axon population counted by experimenter 1. The axon size distributions for the unmyelinated fibers are shown in Figures 15, 16, and 17. Unmyelinated fibers ranged in size from 0.17-1.24 microns with a mean fiber size of 0.50 microns (mode = 0.41). The statistically significant difference found between the unmyelinated fiber populations counted in the peripheral (n = 239) and central (n = 143) optic nerve regions may reflect a sampling error to some degree. Unmyelinated axons are more easily and reliably identified in the central region of the optic nerve because of the higher density of astrocyte processes and nuclei. The dense orthogonal arrays of astrocyte foot processes in the peripheral region of the optic nerve makes distinguishing unmyelinated fibers from other processes very difficult. If the unmyelinated axons do, in fact, have an anatomical affinity for astrocyte paranuclear regions, then the population difference between central and peripheral optic nerve is reasonable since astrocyte nuclei do appear to be more numerous in the central region.

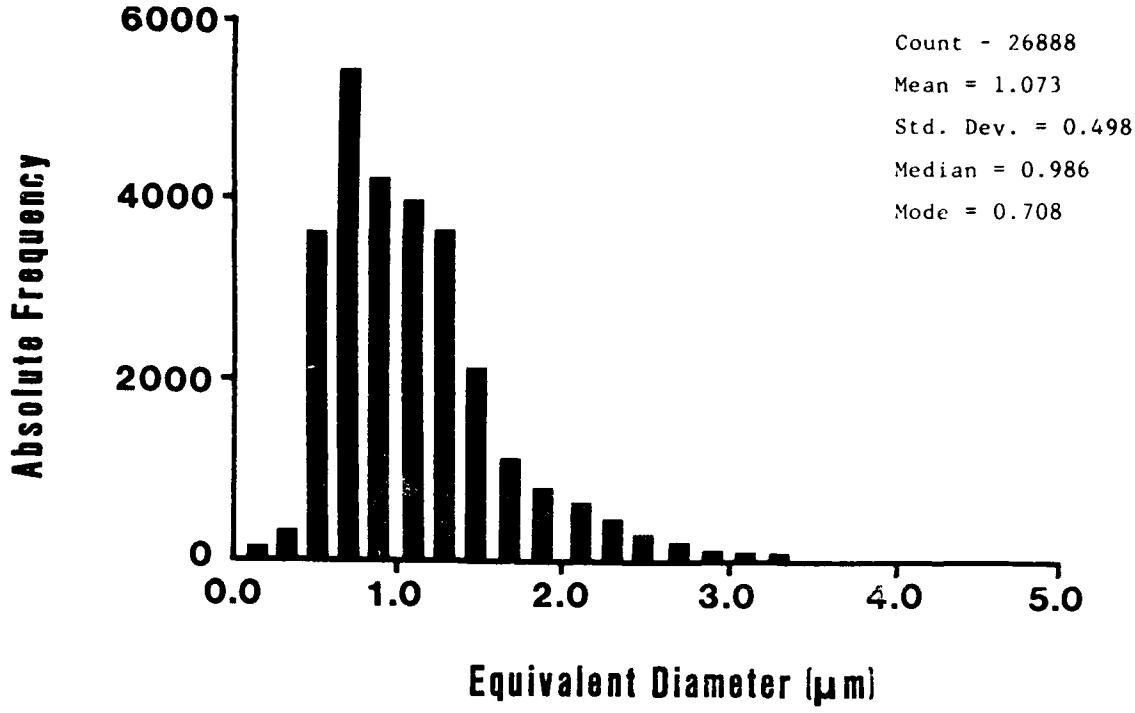

CLASSIFICATION LIST

UNDERFLOW = 0 OVERFLOW = 0 FREQUENCIES

CLASS	FROM	TO	ABS	REL %	CUM. ABS.	CUM. REL. %
1	0.00	0.20	60	.22	60	.22
2	0.20	0.40	331	1.23	391	1.45
3	0.40	0.60	3682	13.69	4073	15.15
4	0.60	0.80	5453	20.28	9526	35.43
5	0.80	1.00	4221	15.70	13747	51.13
6	1.00	1.20	3999	14.87	17746	66.00
7	1.20	1.40	3636	13.52	21382	79.52
8	1.40	1.60	2127	7.91	23509	87.43
9	1.60	1.80	1074	3.99	24583	91.43
10	1.80	2.00	745	2.77	25328	94.20
11	2.00	2.20	590	2.19	25918	96.39
12	2.20	2.40	401	1.49	26319	97.88
13	2.40	2.60	256	.95	26575	98.84
14	2.60	2.80	149	.55	26724	99.39
15	2.80	3.00	73	.27	26797	99.66
16	3.00	3.20	35	.13	26832	99.79
17	3.20	3.40	19	.07	26851	99.86
18	3.40	3.60	12	.04	26863	99.91
19	3.60	3.80	11	.04	26874	99.95
20	3.80	4.00	5	.02	26879	99.97
21	4.00	4.20	6	.02	26885	99.99
22	4.20	4.40	3	.01	26888	100.00

FIGURE 8. Myelinated axons - combined data.

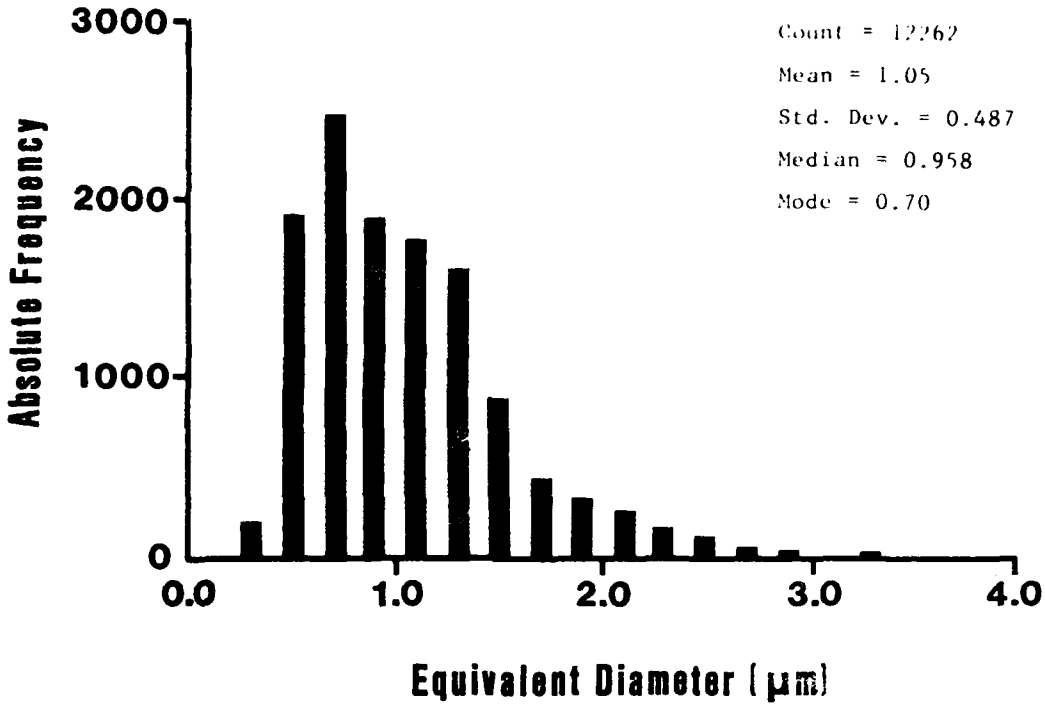

CLASSIFICATION LIST

UNDERFLOW = 0		OVERFLOW = 3		FREQUENCIES		
CLASS	FROM	TO	ABS	REL%	CUM. ABS.	CUM. REL.%
1	0.0	0.2	0	0.00	0	0.00
2	0.2	0.4	188	1.53	188	1.53
3	0.4	0.6	1918	15.64	2106	17.18
4	0.6	0.8	2509	20.46	4615	37.64
5	0.8	1.0	1912	15.59	6527	53.23
6	1.0	1.2	1792	14.61	8319	67.84
7	1.2	1.4	1632	13.31	9951	81.15
8	1.4	1.6	893	7.28	10844	88.44
9	1.6	1.8	450	3.67	11294	92.11
10	1.8	2.0	322	2.63	11616	94.73
11	2.0	2.2	260	2.12	11876	96.85
12	2.2	2.4	158	1.29	12034	98.14
13	2.4	2.6	104	.85	12138	98.99
14	2.6	2.8	51	.42	12189	99.40
15	2.8	3.0	35	.29	12224	99.69
16	3.0	3.2	15	.12	12239	99.81
17	3.2	3.4	8	.07	12247	99.88
18	3.4	3.6	3	.02	12250	99.90
19	3.6	3.8	5	.04	12255	99.94
20	3.8	4.0	4	.03	12259	99.98

FIGURE 9. Myelinated axons - experimenter 1 total sample.

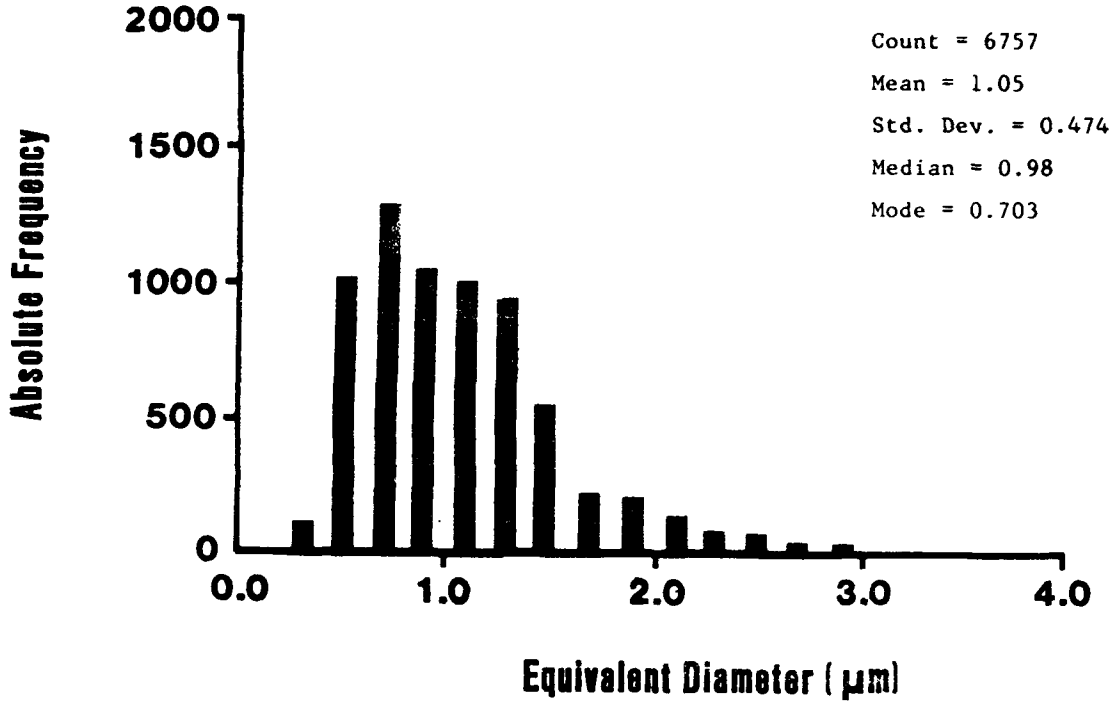

CLASSIFICATION LIST

UNDERFLOW = 0		OVERFLOW = 0		FREQUENCIES		
CLASS	FROM	TO	ABS	REL %	CUM. ABS.	CUM. REL.%
1	0.0	0.2	0	0.00	0	0.00
2	0.2	0.4	109	1.61	109	1.61
3	0.4	0.6	1016	15.04	1125	16.65
4	0.6	0.8	1299	19.22	2424	35.87
5	0.8	1.0	1059	15.67	3483	51.55
6	1.0	1.2	1021	15.11	4504	66.66
7	1.2	1.4	954	14.12	5458	80.78
8	1.4	1.6	552	8.17	6010	88.94
9	1.6	1.8	221	3.27	6231	92.22
10	1.8	2.0	199	2.95	6430	95.16
11	2.0	2.2	134	1.98	6564	97.14
12	2.2	2.4	77	1.14	6641	98.28
13	2.4	2.6	59	.87	6700	99.16
14	2.6	2.8	32	.47	6732	99.63
15	2.8	3.0	16	.24	6748	99.87
16	3.0	3.2	4	.06	6752	99.93
17	3.2	3.4	3	.04	6755	99.97
18	3.4	3.6	0	0.00	6755	99.97
19	3.6	3.8	2	.03	6757	100.00

FIGURE 10. Myelinated axons - experimenter 1 central optic nerve.

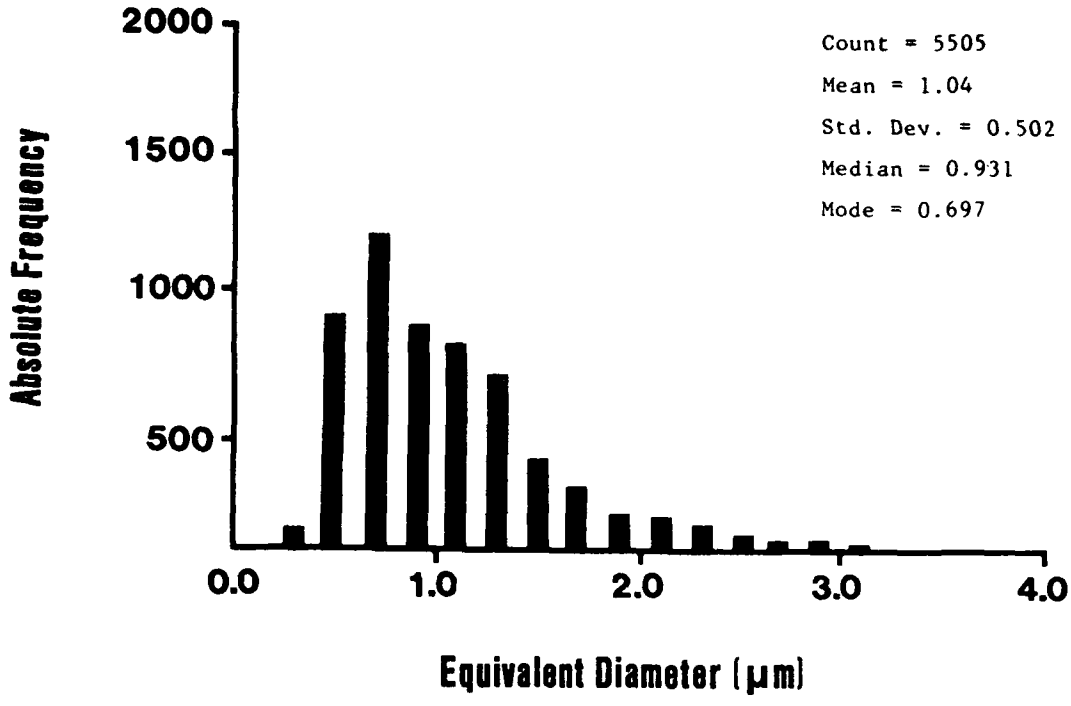

CLASSIFICATION LIST

UNDERFLOW = 0 OVERFLOW = 3 FREQUENCIES

CLASS	FROM	TO	ABS	REL %	CUM. ABS.	CUM. REL. %
1	0.0	0.2	0	0.00	0	0.00
2	0.2	0.4	79	1.44	79	1.44
3	0.4	0.6	902	16.39	981	17.82
4	0.6	0.8	1210	21.98	2191	39.80
5	0.8	1.0	853	15.50	3044	55.30
6	1.0	1.2	771	14.01	3815	69.30
7	1.2	1.4	678	12.32	4493	81.62
8	1.4	1.6	341	6.19	4834	87.81
9	1.6	1.8	229	4.16	5063	91.97
10	1.8	2.0	123	2.23	5186	94.21
11	2.0	2.2	126	2.29	5312	96.49
12	2.2	2.4	81	1.47	5393	97.97
13	2.4	2.6	45	.82	5438	98.78
14	2.6	2.8	19	.35	5457	99.13
15	2.8	3.0	19	.35	5476	99.47
16	3.0	3.2	11	.20	5487	99.67
17	3.2	3.4	5	.09	5492	99.76
18	3.4	3.6	3	.05	5495	99.82
19	3.6	3.8	3	.05	5498	99.87
20	3.8	4.0	4	.07	5502	99.95

FIGURE 11. Myelinated axons - experimenter 1 peripheral optic nerve.

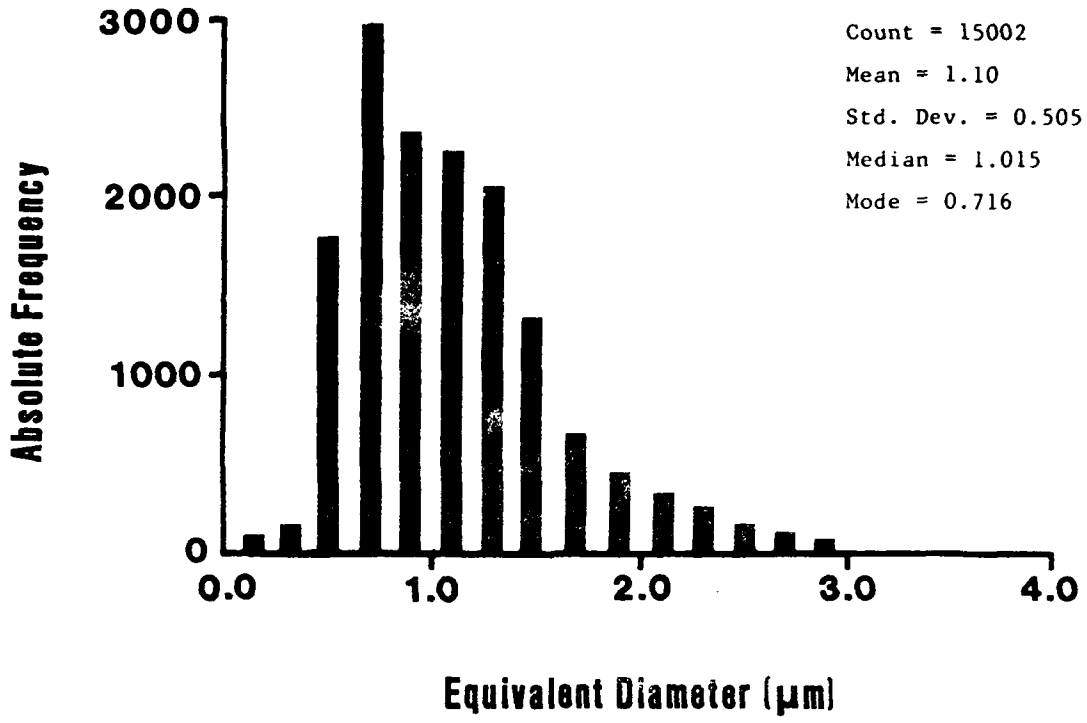

CLASSIFICATION LIST

UNDERFLOW = 0 OVERFLOW = 6 FREQUENCIES

CLASS	FROM	TO	ABS	REL %	CUM. ABS.	CUM. REL. %
1	0.0	0.2	60	.40	60	.40
2	0.2	0.4	143	.95	203	1.35
3	0.4	0.6	1781	11.87	1984	13.22
4	0.6	0.8	2987	19.91	4971	33.14
5	0.8	1.0	2358	15.72	7329	48.85
6	1.0	1.2	2249	14.99	9578	63.84
7	1.2	1.4	2057	13.71	11635	77.56
8	1.4	1.6	1296	8.64	12931	86.20
9	1.6	1.8	674	4.49	13605	90.69
10	1.8	2.0	445	2.97	14050	93.65
11	2.0	2.2	339	2.26	14389	95.91
12	2.2	2.4	249	1.66	14638	97.57
13	2.4	2.6	159	1.06	14797	98.63
14	2.6	2.8	101	.67	14898	99.31
15	2.8	3.0	41	.27	14939	99.58
16	3.0	3.2	23	.15	14962	99.73
17	3.2	3.4	14	.09	14976	99.83
18	3.4	3.6	9	.06	14985	99.89
19	3.6	3.8	8	.05	14993	99.94
20	3.8	4.0	3	.02	14996	99.96

FIGURE 12. Myelinated axons - experimenter 2 total sample.

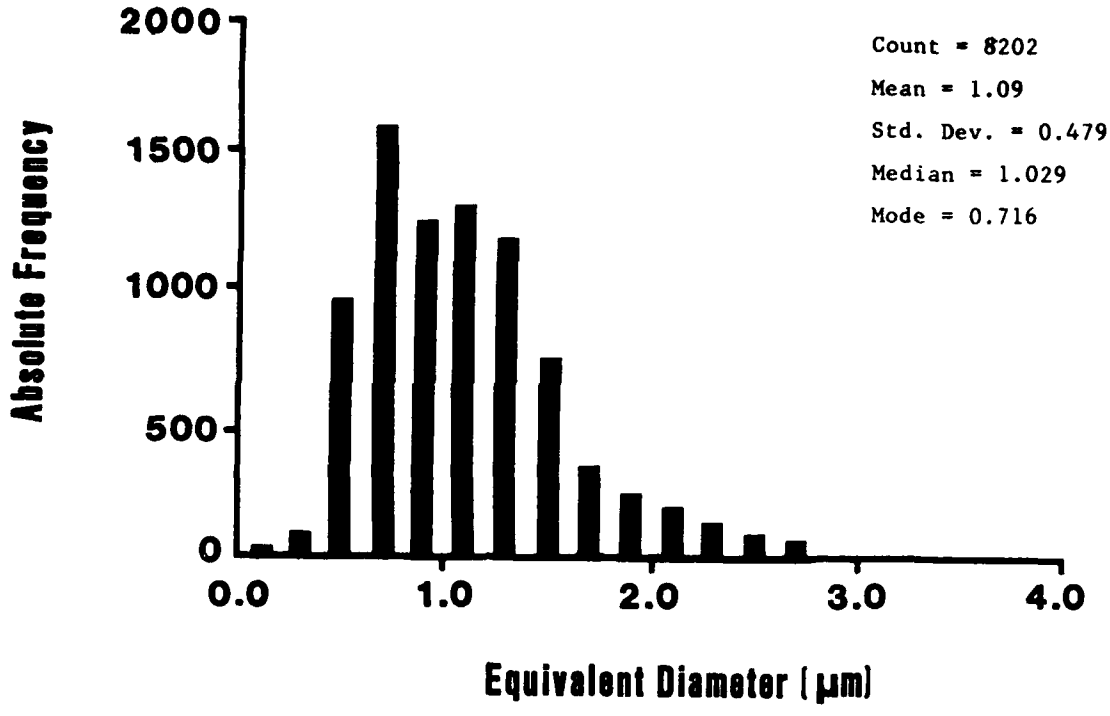

CLASSIFICATION LIST

UNDERFLOW = 0		OVERFLOW = 0			FREQUENCIES	
CLASS	FROM	TO	ABS	REL %	CUM. ABS.	CUM. REL.%
1	0.0	0.2	24	.29	24	.29
2	0.2	0.4	74	.90	98	1.19
3	0.4	0.6	950	11.58	1048	12.78
4	0.6	0.8	1602	19.53	2650	32.31
5	0.8	1.0	1257	15.33	3907	47.63
6	1.0	1.2	1326	16.17	5233	63.80
7	1.2	1.4	1190	14.51	6423	78.31
8	1.4	1.6	745	9.08	7168	87.39
9	1.6	1.8	330	4.02	7498	91.42
10	1.8	2.0	237	2.89	7735	94.31
11	2.0	2.2	179	2.18	7914	96.49
12	2.2	2.4	124	1.51	8038	98.00
13	2.4	2.6	84	1.02	8122	99.02
14	2.6	2.8	56	.68	8178	99.71
15	2.8	3.0	12	.15	8190	99.85
16	3.0	3.2	7	.09	8197	99.94
17	3.2	3.4	1	.01	8198	99.95
18	3.4	3.6	3	.04	8201	99.99
19	3.6	3.8	1	.01	8202	100.00

FIGURE 13. Myelinated axons - experimenter 2 central optic nerve.

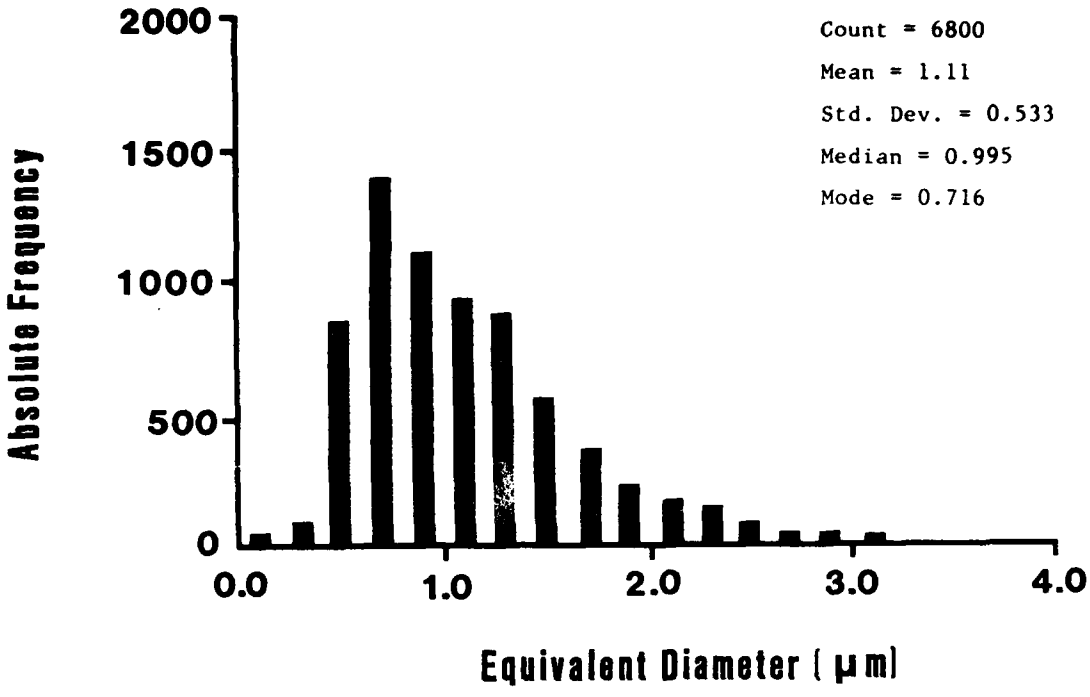

CLASSIFICATION LIST

UNDERFLOW = 0		OVERFLOW = 6		FREQUENCIES		
CLASS	FROM	TO	ABS	REL %	CUM. ABS.	CUM. REL.
1	0.0	0.2	36	.53	36	.53
2	0.2	0.4	69	1.01	105	1.54
3	0.4	0.6	831	12.22	936	13.76
4	0.6	0.8	1385	20.37	2321	34.13
5	0.8	1.0	1101	16.19	3422	50.32
6	1.0	1.2	923	13.57	4345	63.90
7	1.2	1.4	867	12.75	5212	76.65
8	1.4	1.6	551	8.10	5763	84.75
9	1.6	1.8	344	5.06	6107	89.81
10	1.8	2.0	208	3.06	6315	92.87
11	2.0	2.2	160	2.35	6475	95.22
12	2.2	2.4	125	1.84	6600	97.06
13	2.4	2.6	75	1.10	6675	98.16
14	2.6	2.8	45	.66	6720	98.82
15	2.8	3.0	29	.43	6749	99.25
16	3.0	3.2	16	.24	6765	99.49
17	3.2	3.4	13	.19	6778	99.68
18	3.4	3.6	6	.09	6784	99.76
19	3.6	3.8	7	.10	6791	99.87
20	3.8	4.0	3	.04	6794	99.91

FIGURE 14. Myelinated axons - experimenter 2 peripheral optic nerve.

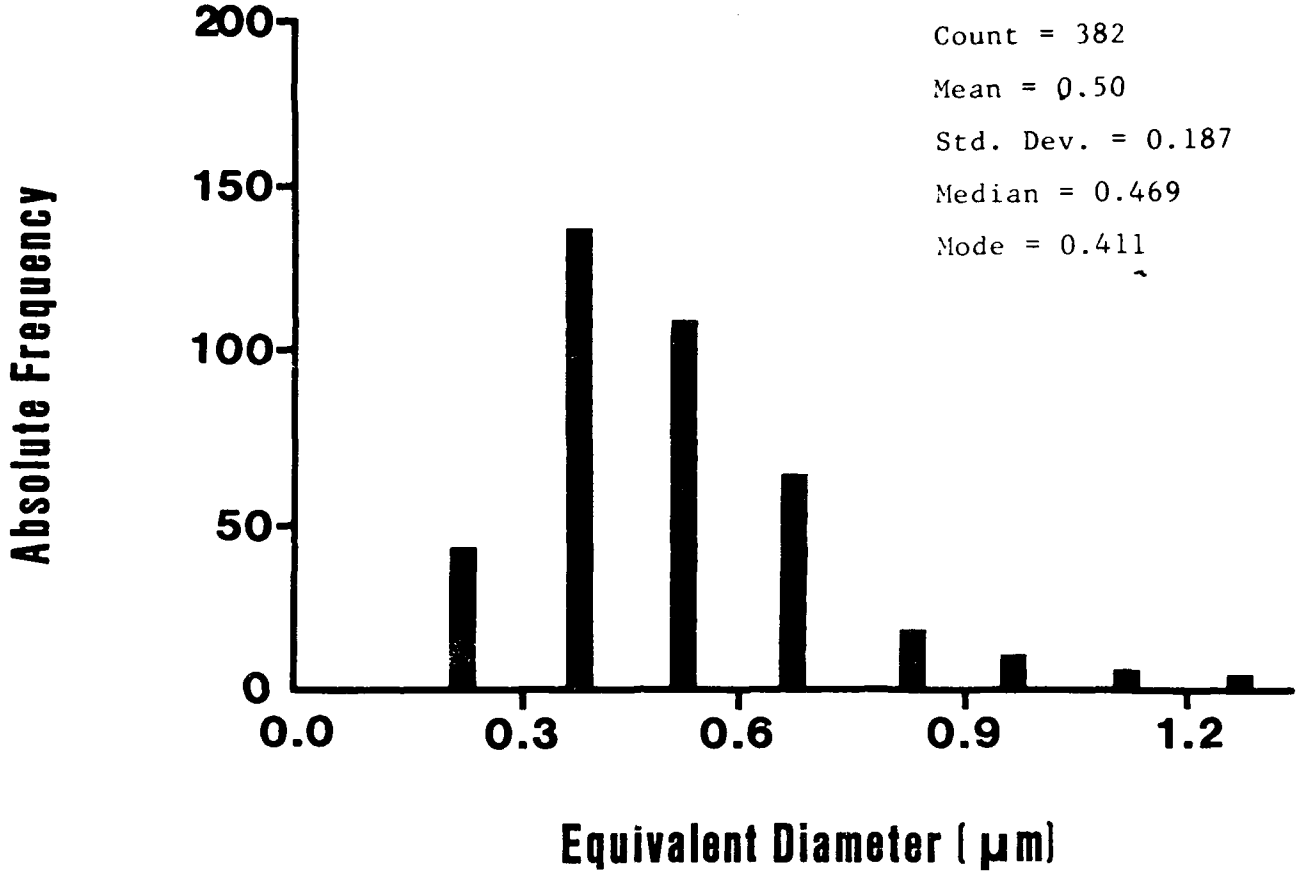

CLASSIFICATION LIST

UNDERFLOW = 0		OVERFLOW = 0		FREQUENCIES		
CLASS	FROM	TO	ABS	REL %	CUM. ABS.	CUM. REL.%
1	0.00	0.15	0	0.00	0	0.00
2	0.15	0.30	40	10.47	40	10.47
3	0.30	0.45	137	35.86	177	46.34
4	0.45	0.60	109	28.53	286	74.87
5	0.60	0.75	63	16.49	349	91.36
6	0.75	0.90	17	4.45	366	95.81
7	0.90	1.05	10	2.62	376	98.43
8	1.05	1.20	4	1.05	380	99.48
9	1.20	1.35	2	.52	382	100.00

FIGURE 15. Unmyelinated axons - experimenter 1 total sample.

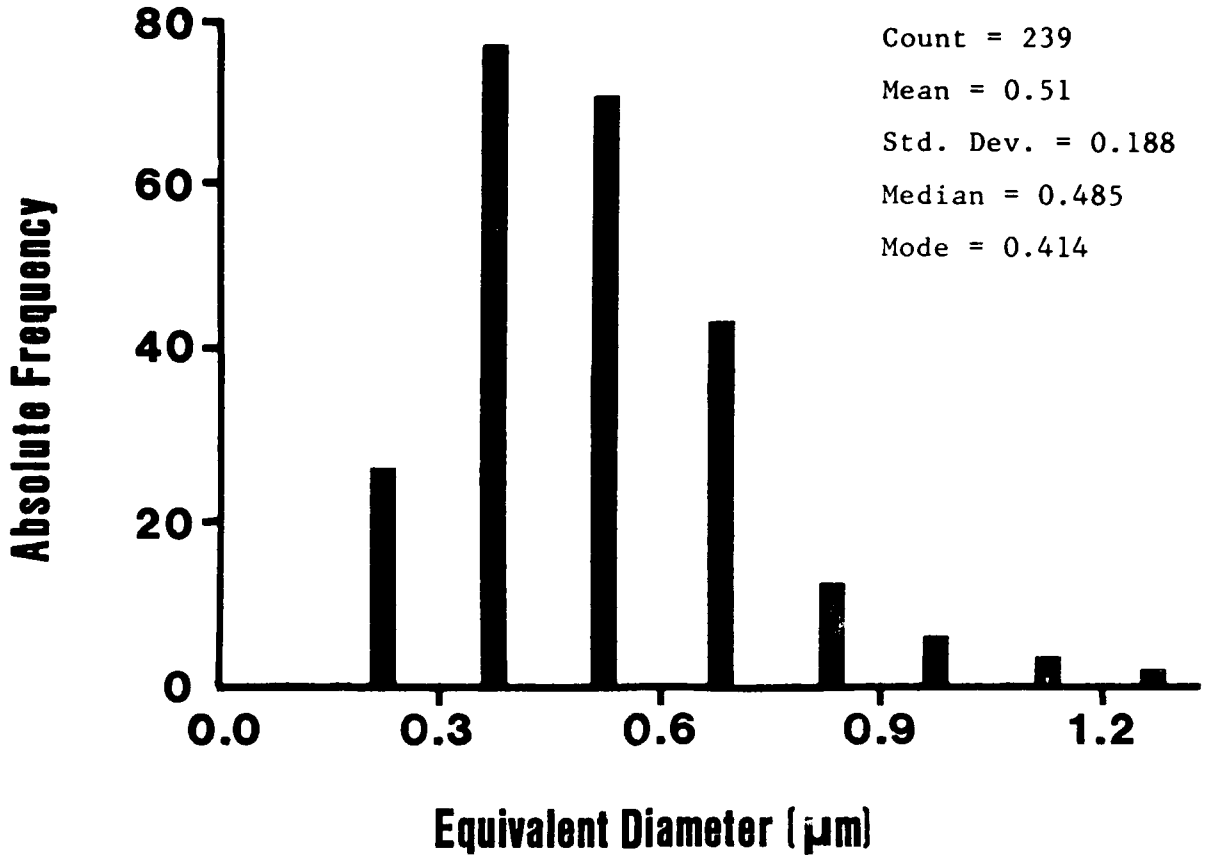

CLASSIFICATION LIST

UNDERFLOW = 0 OVERFLOW = 0 FREQUENCIES

CLASS	FROM	TO	ABS	REL %	CUM. ABS.	CUM. REL. %
1	0.00	0.15	0	0.00	0	0.00
2	0.15	0.30	26	10.88	26	10.88
3	0.30	0.45	77	32.22	103	43.10
4	0.45	0.60	71	29.71	174	72.80
5	0.60	0.75	43	17.99	217	90.79
6	0.75	0.90	12	5.02	229	95.82
7	0.90	1.05	6	2.51	235	98.33
8	1.05	1.20	3	1.26	238	99.58
9	1.20	1.35	1	.42	239	100.00

FIGURE 16. Unmyelinated axons - experimenter 1 central optic nerve.

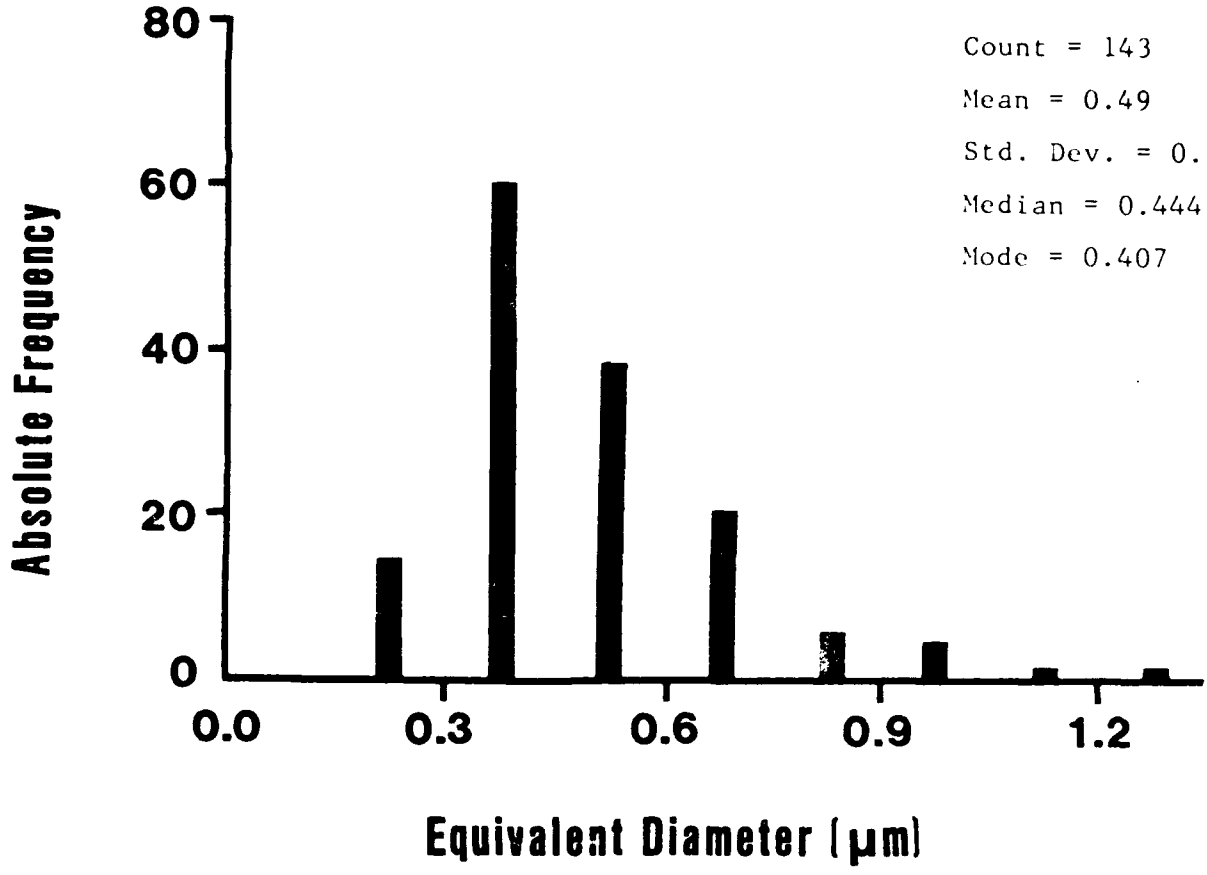

CLASSIFICATION LIST

UNDERFLOW = 0 OVERFLOW = 0 FREQUENCIES

CLASS	FROM	TO	ABS	REL %	CUM. ABS.	CUM. REL.%
1	0.00	0.15	0	0.00	0	0.00
2	0.15	0.30	14	9.79	14	9.79
3	0.30	0.45	60	41.96	74	51.75
4	0.45	0.60	38	26.57	112	78.32
5	0.60	0.75	20	13.99	132	92.31
6	0.75	0.90	5	3.50	137	95.80
7	0.90	1.05	4	2.80	141	98.60
8	1.05	1.20	1	.70	142	99.30
9	1.20	1.35	1	.70	143	100.00

FIGURE 17. Unmyelinated axons - experimenter 1 peripheral optic nerve.

DISCUSSION

The results of this study are consistent with previous optic nerve studies on other vertebrates in the expected high percentage of myelinated fibers, the equivalent diameter size distributions, and axon density. All of the studies that have reported axon size distributions generally have found axons to fall within the range of 0.2-4.0 microns in diameter. This study has a considerable advantage over most previous studies due to the use of a highly sophisticated computer image analysis system to collect and analyze data. In particular, equivalent diameters were calculated directly from traced axon areas rather than having to subjectively match the obliquely-shaped axons with circle templates as most previous studies on optic nerve have done.

Since a comprehensive comparative study or review of optic nerve studies across vertebrates has not been undertaken, a summary of previous findings on fiber counts and axon size distributions is given in Table 2. Many earlier optic nerve studies used only light microscopy (Bruesch and Arey, 1942; Donovan, 1967). However, only those optic nerve studies employing electron microscopy have been discussed in this paper and are included in the table. Not all of the studies gave complete information on axon size distributions. Hence, some figures in the table are extrapolated from data provided in the results section of the reference. Myelinated axon size distributions do not compare well because some studies made their measurements from the outside of the myelin sheath while most measured size from inside the myelin sheath.

The anatomical observations in this study yielded some interesting ontogenetic or developmental trends among vertebrates, from amphibia to primates, as they proceed up the phylogenetic scale. In general, some of the following comparative observations on the anatomical organization of the optic nerve can be made. Amphibia have very few myelinated axons (Maturana, 1959; Fulbrook, personal observations); primates have few or no unmyelinated axons. Amphibia have few oligodendrocytes and many astrocytes; primates have approximately equal numbers of oligodendrocytes and astrocytes. The larger the optic nerve and greater the number of myelinated axons, the greater the amount of connective tissue and blood vessel invaginations into the nerve. Amphibia generally have blood vessels around their optic nerves, not within. These factors are interrelated when the following facts are considered: the diffusion limit of metabolites from blood vessels is estimated to be a maximum of 200 microns (Prosser, 1973), oligodendrocytes give rise to and maintain myelin sheaths, and astrocytes are well-known for having structural, storage, and metabolite-exchange functions (Blunt, Wendell-Smith, and Baldwin, 1965). Astrocytes appear to function as the blood-brain barrier in the optic nerve.

In this study, the number of axons in the bushbaby optic nerve is estimated to be 384,500. This is in sharp distinction to the total fiber counts found in humans (1.2-1.3 million: Potts, et al., 1972a,b) or rhesus monkey (1.4-1.8 million: Potts, et al., 1972a,b; Ogden and Miller, 1966). Extrapolating data on total counts and total area from the Potts, et al. (1972a,b)

TABLE 2. COMPARATIVE SUMMARY OF OPTIC NERVE STUDIES

VERTEBRATES	STUDY	FIBER COUNTS TOTAL	FIBER COUNTS % UNMYELINATED	AXON SIZE DISTRIBUTIONS (MICRONS) MYELINATED (MODE)	AXON SIZE DISTRIBUTIONS (MICRONS) UNMYELINATED (MODE)
Human	Potts et al., 1972a,b	1.1-1.3 million	None	~0.2-4.8 (0.25-0.50)	None
Rhesus Monkey	Potts et al., 1972a,b	1.5-1.8 million	None	~0.2-4.8 (0.25-0.50)	None
Rhesus Monkey	Ogden & Miller, 1966	1.4 million	None	0.4-6.0 (1.2)*	None
Galago	Present Study	385,000	2.8	0.2-4.3 (0.7)	0.18-1.25 (0.41)
Rabbit	Vaney & Hughes, 1976	394,000	2	0.25-7.0 (0.75)	Not given
Cat	Stone & Campion, 1978	128,600	None	Not given	None
Cat	Hughes & Wassle, 1976	193,000	None	0.5-13.5 (1.0)*	None
Golden Hamster	Rhoades, Hsu, & Parfett, 1979	110,000	3.6	0.2-3.93 (1.2)*	0.2-1.0 (0.63)
Golden Hamster	Tiao & Blakemore, 1976	119,000	58	0.4-1.7 (0.9)	0.2-1.0 (0.3)
Pigmented Rat	Hughes, 1977	120,000	None	0.4-5.2 (1.0)*	None
Albino Rat	Forrester & Peters, 1967	117,000	None	0.4-4.0 (1.0)*	None
Opossum	Hokoc & Oswaldo-Cruz, 1978	74,700	20	0.5-7.0 (1.25)*	0.25-2.25 (0.75)
Opossum	Kirby et al., 1982	100,000	2	0.2-6.0 (0.7)	0.2-1.6 (0.6)
Pigeon	Duff & Scott, 1979	2.3 million	15-25	0.3-4.0 (0.75)	Not given
Pigeon	Binggelli & Paule, 1969	2.4 million	29	0.5-4.0 (<1.0)	0.1-0.7 (~0.4)
Duck	O'Flaherty, 1971	1.5 million	None	0.3-6.0 (1.15)*	None
Turtle	Fulbrook & Granda, 1978	790,000	25	0.4-4.0 (<1.0)	0.2-1.0 (<0.6)
Eugerres (Fish)	Tapp, 1973, 1974	200,000	2.5	0.2-7.6 (0.7)	Not given
Anurans (Frog)	Maturana, 1959, 1960	485,000	97	0.7-5.0 (<1.5)	0.15-0.6 (0.2-0.3)
Xenopus	Gaze & Peters, 1961	34,250	82	0.5-4.0 (1.5)	0.1-1.2 (0.4)
Xenopus	Wilson, 1971	52,000	87	0.3-3.0 (1.5)	0.1-2.0 (0.2)

*Axon size distributions measured around outside of myelin sheath.

study, however, yields comparable fiber densities with the bushbaby. The optic nerve in a human, for instance, is approximately 2.7 mm in diameter compared to approximately 1.3 mm for the bushbaby. This result compares better than the extrapolated data from a cat which would have a fiber density of approximately 206 fibers per 100 μm^2 (Stone and Campion, 1978), compared to 376 fibers per 1000 μm^2 found here.

These results contribute additional information on the anatomical organization of the visual system in the bushbaby, Galago crassicaudatus. Recently, DeBruyn, Wise, and Casagrande (1980) published a study on the size and topographic arrangement of retinal ganglion cells in the galago. A differential density distribution was found ranging from a high in the area centralis (12,000 cells/mm^2) to a low in the periphery (300 cells/mm^2). Unfortunately, estimates of the total retinal area or total cell counts were not made and their results cannot be directly compared to ours. Significant correlations have been found between the physiological properties of retinal ganglion cells with their size, morphology, density, and distribution (Rowe and Stone, 1976; Nelson, Famiglietti, and Kolb, 1977; Hsiao, Watanabe, and Fukuda, 1984). In addition, vertebrates with regions of retinal specialization and high ganglion cell densities have been found to possess greater acuity (Rolls and Cowey, 1970). The density and total count of optic nerve fibers found here, along with the comparatively wide range of fiber sizes indicates that the galago possesses a highly developed visual system at the retinal level regardless of its probable weakness in photopic vision.

The DeBruyn, Wise and Casagrande (1980) study is one of the first to explore the retinal cells of the bushbaby. In addition, Stone and Johnston (1981) published a comparative study on retinal topography which included the bushbaby. More recent studies on the photoreceptor population also have been undertaken (Hope and Ulshafer, 1984; Fulbrook, unpublished data). Much information already is available on the central visual pathways and their physiological properties (Casagrande and DeBruyn, 1982). This area of research has continued with published articles on the laminar organization of receptive field properties in the lateral geniculate nucleus of bushbaby (Norton and Casagrande, 1982), the organization of cortical visual areas (Allman and McGuinness, 1983), and on the interhemisphere connections of visual cortex in galagos (Cusick, Gould, and Kaas, 1984). Much study on the visual system of galago still needs to be done, even though the amount of information known about this animal likely never will equal that of other established vertebrates (e.g., cat and turtle). For this field of research, however, the bushbaby does appear to be highly suitable for additional study for its usefulness in comparative research and as a scotopic model of human visual system function.

REFERENCES

Allman, J.M., and McGuinness, E. 1983. The organization of cortical visual areas in a strepsirhine primate, Galago senegalensis. Proceedings of the Society of Neuroscience. 9:957 (Abstract).

Binggelli, R.L., and Paule, N.J. 1969. The pigeon retina: qualitative aspects of the optic nerve and ganglion cell layer. Journal of Comparative Neurology. 137:1-18.

Blunt, M.J., Wendell-Smith, C.P., and Baldwin, F. 1965. Glia nerve fiber relationships in mammalian optic nerve. Journal of Anatomy. 99:1-11.

Bruesch, S.R., and Arey, L.B. 1942. The number of unmyelinated fibers in the optic nerve of vertebrates. Journal of Comparative Neurology. 77:631-665.

Bunt, S.M., and Horder, T.J. 1983. Evidence for an orderly arrangement of optic axons within the optic nerves of the major nonmammalian vertebrate classes. Journal of Comparative Neurology. 213:94-114.

Casagrande, V.A., and DeBruyn, E.J. 1982. The galago visual system: aspects of normal organization and developmental plasticity. In D.E. Haines (ed.): The Lesser Bushbaby as a Laboratory Animal. Cleveland, C.R. C. Press.

Cohen, A. 1972. Rods and cones. In M.G.F. Fuortes (ed.): Handbook of Sensory Physiology II: Physiology of Photoreceptor Organs. New York, Springer-Verlag.

Cusick, C.G., Gould, H.J., III., and Kaas, J.H. 1984. Interhemisphere connections of visual cortex of owl monkeys (Aotus trivirgatus), Marmosets (Callithrix jacchus), and galagos (Galagos crassicaudatus). Journal of Comparative Neurology. 230:311-336.

Dartnall, J.H.A., Arden, G.B., Ikeda, H., Luck, C.P., Rosenberg, M.E., Pedler, C.M.H., and Tansley, K. 1965. Anatomical, electrophysiological and pigmentary aspects of vision in the bushbaby, an interpretative study. Vision Research. 5:399-424.

DeBruyn, E.J., Wise, V.L., and Casagrande, V.A. 1980. The size and topographic arrangement of retinal ganglion cells in the galago. Vision Research. 20:315-327.

Donovan, A. 1967. The nerve fibre composition of the cat optic nerve. Journal of Anatomy. 101:1-11.

Dowling, J.E., and Ripps, H. 1970. Visual adaptation in the retina of the skate. Journal of General Physiology. 56:491-520.

Duff, T.A., and Scott, G. 1979. Electron microscopic evidence of a ventronasal to dorsotemporal variation in fiber size in pigeon optic nerve. Journal of Comparative Neurology. 183:679-687.

Dunlap, S.A., and Beazley, L.D. 1984. A morphometric study of the retinal ganglion cell layer and optic nerve from metamorphosis in Xenopus laevis. Vision Research. 24:417-427.

Epstein, M.A., and Holt, S.J. 1963. The localization by electron microscopy of Hela cell surface enzyme spitting ATP. Journal of Cellular Biology. 19:325.

Forrester, J., and Peters, A. 1967. Nerve fibres in the optic nerve of the rat. Nature. 214:245-247.

Fulbrook, J.E. Personal observations.

Fulbrook, J.E. Unpublished data.

Fulbrook, J.E., and Granda, A.M. 1978. The anatomy of the optic nerve of the turtle, Pseudemys scripta elegans. Proceedings of the Society for Neuroscience. 4:628 (Abstract).

Gaze, R.M., and Peters, A. 1961. The development, structure and composition of the optic nerve of Xenopus laevis (Daudin). Quarterly Journal of Experimental Physiology. 46:299-309.

Granda, A.M., and Dvorak, C.A. 1977. Vision in turtles. In F. Crescitelli (ed.): Handbook of Sensory Physiology, Vol. VII/5. The Visual System in Vertebrates. New York, Springer-Verlag.

Green, D.G. 1973. Scotopic and photopic components of the rat electroretinogram. Journal of Physiology. 228:791-797.

Green, D.G., Dowling, J.E., Siegel, I.M., and Ripps, H. 1975. Retinal mechanisms of visual adaptation in the skate. Journal of General Physiology. 65:483-502.

Grusser, O.J., and Grusser-Cornehls, U. 1976. Neurophysiology of the anuran visual system. In R. Linas and W. Precht (eds.): Frog Neurobiology. New York, Springer-Verlag.

Harding, T.H., and Enroth-Cugell, C. 1978. Absolute dark sensitivity and center size in cat retinal ganglion cells. Brain Research. 153:157-162.

Hokoc, J.N., and Oswaldo-Cruz, E. 1978. Quantitative anlaysis of the opossum's optic nerve: an electron microscope study. Journal Comparative Neurology. 178:773-782.

Hope, G.M., and Ulshafer, R.J. 1984. Characterization of the Photoreceptor Population of the Retina of Bushbaby. Ft. Detrick, MD: U.S. Army Medical Research and Development Command (DAMD17-83-C-3066).

Hsiao, C.F., Watanabe, M., and Fukuda, Y. 1984. The relation between axon diameter and axonal conduction velocity of Y, X, and W cells in the cat retina. Brain Research. 309:357-361.

Hughes, A. 1977. The pigmented-rat optic nerve: fiber count and fiber diameter spectrum. Journal of Comparative Neurology. 176:263-267.

Hughes, A., and Wassle, H. 1976. The cat optic nerve: fiber total count and diameter spectrum. Journal of Comparative Neurology. 169:171-184.

Hyatt, M.A. 1981. Principles and Techniques of Electron Microscopy: Biological Applications. Baltimore, University Park Press.

Kirby, M.A., Cliff-Forsberg, L., Wilson, P.D., and Rapisardi, S.C. 1982. Quantitative analysis of the optic nerve of the North American opossum (Didelphis virginiana): an electron microscope study. Journal of Comparative Neurology. 211:318-327.

Maturana, H.R. 1959. Number of fibres in the optic nerve and the number of ganglion cells in the retina of anurans. Nature. 183:1406-1407.

Maturana, H.R. 1960. The fine anatomy of the optic nerve of anurans - an electron microscope study. Journal of Biophysical and Biochemical Cytology. 7:107-119.

Nelson, R., Famiglietti, E., and Kolb, H. 1977. On-center and off-center ganglion cells branch at different levels in the cat inner plexiform layer. ARVO Abstract. 44.

Norton, T.T., and Casagrande, V.A. 1982. Laminar organization of receptive-field properties in lateral geniculate nucleus of bushbaby (Galago crassicaudatus). Journal of Neurophysiology. 47(4):715-741.

O'Flaherty, J.J. 1971. The optic nerve of the mallard duck: fiber-diameter frequency distribution and physiological properties. Journal of Comparative Neurology. 143:17-24.

Ogden, T.E., and Miller, R.F. 1966. Studies of the optic nerve of the Rhesus monkey: nerve fiber spectrum and physiological properties. Vision Research. 6:485-506.

Peters, A. 1966. The node of Ranvier in the central nervous system. Quarterly Journal of Experimental Physiology. 51:229-236.

Peters, A., Palay, S., and Webster, H.F. 1970. The Fine Structure of the Nervous System: The Cells and Their Processes. New York: Harper and Row.

Potts, A.M., Hodges, D., Shelman, C.B., Fritz, K.J., Levy, N.S., and Mangnall, Y. 1972a. Morphology of the primate optic nerve. I. Method and total fiber count. Investigative Ophthalmology. 11:980-988.

Potts, A.M., Hodges, D., Shelman, C.B., Fritz, K.J., Levy, N.S., and Mangnall, Y. 1972b. Morphology of the primate optic nerve. II. Total fiber size distribution and fiber density distribution. Investigative Ophthalmology. 11:989-1003.

Prosser, C.L. 1973. Comparative Animal Physiology. Philadelphia, P.A.: W.B. Sanders Company.

Reynolds, E.S. 1963. The use of lead citrate at high pH as an electron opaque stain in electron microscopy. Journal of Cellular Biology. 17:208.

Rhoades, R.W., Hsu, L., and Parfett, G. 1979. An electron microscopic analysis of the optic nerve in the golden hamster. Journal of Comparative Neurology. 186:491-504.

Rodieck, R.W. 1973. The Vertebrate Retina: Priciples of Structure and Function. San Francisco, CA: W.H. Freeman and Company.

Rolls, E.T., and Cowey, A. 1970. Topography of the retina and striate cortex and its relationship to visual acuity in rhesus monkeys and squirrel monkeys. Exploratory Brain Research. 10:298-310.

Rowe, M.H., and Stone, J. 1976. Conduction velocity grouping among axons of cat retinal ganglion cells, and their relationship to retinal topography. Experimental Brain Research. 25:339-357.

Stone, J. 1978. The number and distribution of ganglion cells in the cat's retina. Journal of Comparative Neurology. 180:753-772.

Stone, J., and Campion, J.E. 1978. Estimate of the number of myelinated axons in the cat's optic nerve. Journal of Comparative Neurology. 180:799-806.

Stone, J., and Hollander, H. 1971. Optic nerve axon diameters measured in the cat retina: some functional considerations. Experimental Brain Research. 13:498-503.

Stone, J., and Johnston, E. 1981. The topography of primate retina: A study of human, bushbaby and new- and old-world monkeys. Journal of Comparative Neurology. 196:205-223.

Tapp, R.L. 1973. The structure of the optic nerve of the teleost: Eugerres plumieri. Journal of Comparative Neurology. 150: 239-242.

Tapp, R.L. 1974. Axon numbers and distribution, myelin thickness, and the reconstruction of the compound action potential in the optic nerve of the teleost: Eugerres plumieri. Journal of Comparative Neurology. 153:267-274.

Tiao, Y.C., and Blakemore, C. 1976. Regional specialization in the golden hamster's retina. Journal of Comparative Neurology. 168:439-458.

Vaney, D.I., and Hughes, A. 1976. The rabbit optic nerve: fiber diameter spectrum, fiber count, and comparison with retinal cell count. Journal of Comparative Neurology. 170:241-252.

Walls, G.L. 1942. The Vertebrate Eye and Its Adaptive Radiation. Michigan: Cranbrook Press.

Wilson, M.A. 1971. Optic nerve fiber counts and retinal ganglion cell counts during development of Xenopus laevis (Daudin). Quarterly Journal of Experimental Physiology. 65:83-91.

APPENDIX A

Edco Scientific, Incorporated
P.O. Box 3273
Chapel Hill, SC 27514

Polyscience, Incorporated
Paul Valley Industrial Park
Warrington, PA 18976

DuPont Company
Biomedical Products Division
Newtown, CT 06470

Vashaw Scientific, Incorporated
5500 Oakbrook Parkway
Suite 220
Norcross, GA 30093

Ted Pella, Incorporated
P.O. Box 510
Tustin, CA 92680

Carl Zeiss, Incorporated
One Zeiss Drive
Thornwood, NY 10594

Polyscience, Incorporated
Paul Valley Industrial Park
Warrington, PA 18976

INITIAL DISTRIBUTION

Commander
US Army Research Institute of
Environmental Medicine
Natick, MA 01760

Naval Submarine Medical Research
Laboratory
Medical Library, Naval Sub Base
Box 900
Groton, CT 05340

Commander
Naval Air Development Center
Biophysics Lab (ATTN: G. Kydd)
Code 60B1
Warminster, PA 18974

Commanding Officer
Naval Medical Research and
Development Command
National Naval Medical Center
Bethesda, MD 20014

Under Secretary of Defense for
Research and Engineering
ATTN: Military Assistant for
Medical and Life Science
Washington, D.C. 20301

COL Franklin H. Top, Jr., MD
Walter Reed Army Institute
of Research
Washington, D.C. 20307-5100

Commander
U. S. Army Institute of Dental Research
Walter Reed Army Medical Center
Washington, DC 20307-5300

Naval Research Laboratory Library
Code 1433
Washington, DC 20375

Director
US Army Human Engineering Laboratory
ATTN: Technical Library
Aberdeen Proving Ground, MD
21005-5001

US Army Environmental Hygiene
Agency Library
Bldg E2100
Aberdeen Proving Ground, MD 21010

Commander
US Army Medical Research Institute
of Chemical Defense
ATTN: SGRD-UV-AO
Aberdeen Proving Ground, MD
21010-5425

Technical Library
Chemical Research & Development Center
Aberdeen Proving Ground, MD
21010-5423

Commander
US Army Medical Research &
Development Command
ATTN: SGRD-RMS (Ms. Madigan)
Fort Detrick, Frederick, MD
21701-5012

Commander
US Army Medical Research Institute
of Infectious Diseases
Fort Detrick, Frederick, MD 21701

Commander
US Army Medical Bioengineering
Research & Development Laboratory
ATTN: SGRD-UBZ-I
Fort Detrick, Frederick, MD 21701

Dr. R. Newburgh
Director, Biological Sciences Division
Office of Naval Research
600 North Quincy Street
Arlington, VA 22217

Defense Technical Information Center
Cameron Station
Alexandria, VA 22314

Naval Aerospace Medical
Institute Library
Bldg 1953, Code 102
Pensacola, FL 32508

Air University Library
(AUL/LSE)
Maxwell AFB, AL 36112

Chief
Army Research Institute Field Unit
Fort Rucker, AL 36362

Chief
Human Engineering Laboratory
Field Unit
Fort Rucker, AL 36362

AFAMRL/HEX
Wright-Patterson AFB, OH 45433

US Air Force Institute of Technology
(AFIT/LDEE)
Bldg 640, Area B
Wright Patterson AFB, OH 45433

University of Michigan
NASA Center of Excellence
in Man-Systems Research
ATTN: R.G. Snyder, Director
Ann Arbor, MI 48109

Commander
US Army Aviation Systems Command
ATTN: SGRD-UAX-AL (MAJ Lacy)
Bldg 105, 4300 Goodfellow Blvd
St Louis, MO 63120

Commanding Officer
Naval Biodynamics Laboratory
P.O. Box 24907
New Orleans, LA 70189

Commander
US Army Academy of Life Sciences
ATTN: Library
Fort Sam Houston, TX 78234

Commander
US Army Health Services Command
ATTN: HSOP-SO
Fort Sam Houston, TX 78234-6000

Commander
US Army Institute of Surgical Research
ATTN: SGRD-USM (Jan Duke)
Fort Sam Houston, TX 78234-6200

Director of Professional Services
AFMSC/GSP
Brooks Air Force Base, TX 78235

US Air Force School of
Aerospace Medicine
Strughold Aeromedical Library
Documents Section, USAFSAM/TSK-4
Brooks Air Force Base, TX 78235

Commander
Letterman Army Institute of Research
ATTN: Medical Research Library
Presidio of San Francisco, CA 94129

Director
Naval Biosciences Laboratory
Naval Supply Center, Bldg 844
Oakland, CA 94625

Staff Officer, Aerospace Medicine
RAF Staff, British Embassy
3100 Massachusetts Avenue, NW
Washington, DC 20008

Canadian Society of Aviation Medicine
c/o Academy of Medicine, Toronto
Attn: Ms. Carmen King
288 Bloor Street West
Toronto, Ontario M55 1V8

Canadian Forces Medical Liaison Officer
Canadian Defence Liaison Staff
2450 Massachusetts Avenue, NW
Washington, DC 20008

Officer Commanding
School of Operational
& Aerospace Medicine
DCIEM, P.O. Box 2000
1133 Sheppard Avenue West
Downsview, Ontario M3M 3B9